

Constraining Recent Oscillations in Quintessence Models with Euclid

N. A. Lima*

*Astronomy Centre, University of Sussex, Brighton, BN1 9QH, UK
Centro de Astrofísica, Universidade do Porto, Rua das Estrelas, 4150-762 Porto, Portugal*

P. T. P. Viana†

*Centro de Astrofísica, Universidade do Porto, Rua das Estrelas, 4150-762 Porto, Portugal
Departamento de Física e Astronomia, Faculdade de Ciências,
Universidade do Porto, Rua do Campo Alegre, 687, 4169-007 Porto, Portugal*

I. Tereno‡

Centro de Astronomia e Astrofísica da Universidade de Lisboa, Tapada da Ajuda, 1349-018, Lisboa, Portugal

Euclid is a future space-based mission that will constrain dark energy with unprecedented accuracy. Its photometric component is optimized for Weak Lensing studies, while the spectroscopic component is designed for Baryon Acoustic Oscillations (BAO) analysis. We use the Fisher matrix formalism to make forecasts on two quintessence dark energy models with a dynamical equation of state that leads to late-time oscillations in the expansion rate of the Universe. We find that Weak Lensing will place much stronger constraints than the BAO, being able to discriminate between oscillating models by measuring the relevant parameters to 1σ precisions of 5 to 20%. The tight constraints suggest that Euclid data could identify even quite small late-time oscillations in the expansion rate of the Universe.

I. INTRODUCTION

The first evidence for an accelerating Universe was uncovered in 1998 through the luminosity distance-redshift relation obtained for type Ia Supernova [1, 2], and has been consistently corroborated by subsequent observations [3, 4]. This phenomenon rapidly became one of the most intriguing problems in modern Cosmology. Since then, there have been many solutions proposed and some have survived the increasingly tight constraints imposed by observational data and are planned to be analysed by Euclid ¹ data [5]. Among those solutions, which include changes to the left-hand side (or the geometry/gravity part) of Einstein's field equations, as in modified gravity ($f(R)$) theories [6, 7], or the introduction of extra spatial dimensions, as in braneworld models [8], one of the most popular assumes the existence of an exotic form of energy in the Universe, characterized by a negative pressure, known as dark energy. If it exists, then present-day observations suggest it accounts for approximately 75 per cent of the Universe's total energy density, and its pressure-to-density ratio (known as the equation of state, w) is nearly constant with time and close to -1 [9–12] (see Ref. [13] for more details). If future observations continue to point towards a value of w near -1 , then the hypothesis of the dark energy being in the form of a cosmological constant, Λ , will gain strength, demanding for more insight on the theoretical problems raised by such

a scenario (see Ref. [14] for a review). But it is also conceivable that observational data will become more easily reproducible with a value for w close to, but not exactly equal to, -1 , opening the door for alternative hypothesis, such as quintessence theories.

In quintessence theories, the dark energy is assumed to be the result of a scalar field, ϕ , minimally coupled to ordinary matter through gravity. The field evolves in a potential $V(\phi)$ with a canonical kinetic term in its lagrangian, which results in a dark energy equation of state $w \geq -1$, not necessarily constant. These models have already been extensively studied [15–18] and, usually, it is assumed that the evolution of the scalar field is monotonic in a potential that satisfies the typical inflationary slow roll conditions (see Ref. [19] for a review on inflation), as given by:

$$\left(\frac{1}{V} \frac{dV}{d\phi}\right)^2 \ll 1, \quad (1)$$

and

$$\left(\frac{1}{V} \frac{d^2V}{d\phi^2}\right) \ll 1. \quad (2)$$

Under these conditions, the dark energy equation of state will always be close to -1 , and the motion of the field becomes greatly simplified [20], allowing for an analytical expression for w as a function of the scale factor a . The motion of the field will also depend on the present-day values of w and of the dark energy density, Ω_ϕ , where Ω_ϕ is the ratio of the dark energy density, ρ_ϕ , to the universe's critical density, ρ_c .

* n.aguiar-lima@sussex.ac.uk

† viana@astro.fc.up.pt

‡ tereno@fc.ul.pt

¹ <http://www.euclid-ec.org/>

However, the inflationary slow-roll conditions need not necessarily apply to quintessence models. This opens up the possibility of complex scalar field dynamics, allowing for a more dynamical evolution of the dark energy equation of state, while still being on average close to -1 . Here we will be particularly interested in scalar field models where late-time oscillations in the expansion rate of the Universe can arise due to non-standard scalar field dynamics. In this paper, we will focus on two scalar field models for which such behavior is possible. Model I assumes a quadratic potential, where an extra degree of freedom, related to the curvature of the potential at the extremum, is introduced on the evolution of the scalar field [21–23]. More specifically, we consider only the case where the curvature of the potential is such that it enables the field to oscillate around the stable extremum [22].

In the case of Model II, we consider power-law potentials where the minimum is zero. When the scalar field is close to the minimum, oscillations begin, and an effectively constant equation of state arises, averaged over the oscillation period (see [24–26] and references therein). In particular, we consider the case where the field starts evolving monotonically, and only close to today it starts oscillating around the minimum, guaranteeing that the observed cosmic history is not significantly affected [27].

In Sec. II, we review the dynamics of quintessence models and briefly present those on which we focus our attention. Then, in Sec. III, we present the main objectives and properties of the Euclid mission, and discuss the Fisher matrix formalism that will be used to forecast both the Weak Lensing and BAO constraints. In Sec. IV, we determine the fiducial values for the parameters of each quintessence model, using the most recent data available from the Supernova Cosmology Project, and then use the Fisher matrix formalism to determine to what accuracy Euclid will be able to constrain the parameters of the considered quintessence models. In Sec. V, we present some final remarks, establishing a comparison between our results and those obtained for the usual dark energy linear parameters $w_0 - w_a$. Throughout the paper we shall assume the metric signature $[-, +, +, +]$ and natural units of $c = \hbar = 8\pi G = 1$.

II. QUINTESSENCE MODELS

The action for quintessence is given by

$$S = \int d^4x \sqrt{-g} \left(-\frac{1}{4}R + \mathcal{L}_m + \mathcal{L}_\phi \right), \quad (3)$$

where R is the Ricci scalar, \mathcal{L}_m and \mathcal{L}_ϕ are, respectively, the matter and scalar field lagrangians. The field's lagrangian takes the form

$$\mathcal{L}_\phi = -\frac{1}{2}g^{\mu\nu} (\partial_\mu\phi) (\partial_\nu\phi) - V(\phi), \quad (4)$$

where $V(\phi)$ is the field's potential.

The energy-momentum tensor of the field is determined by varying the field's individual action with respect to the metric elements $g^{\mu\nu}$, yielding

$$T_{\mu\nu} = \partial_\mu\phi\partial_\nu\phi - g_{\mu\nu} \left[\frac{1}{2}g^{\alpha\beta} (\partial_\alpha\phi\partial_\beta\phi) + V(\phi) \right]. \quad (5)$$

The line element for a flat, homogeneous and isotropic Universe is given by the Friedmann-Robertson-Walker (FRW) metric:

$$ds^2 = -dt^2 + a^2(t) (dx^2 + dy^2 + dz^2), \quad (6)$$

where a is the scale factor, t is the physical time and x , y and z are the spatial comoving coordinates. Using the FRW metric, and assuming that the field depends very weakly on the spatial coordinates, the quintessence energy density, ρ , and pressure, p , are given by

$$\rho_\phi = -T_0^0 = \frac{1}{2}\dot{\phi}^2 + V(\phi), \quad p_\phi = T_i^i = \frac{1}{2}\dot{\phi}^2 - V(\phi), \quad (7)$$

where the dot represents a derivative in order to the physical time t .

As for the dark energy equation of state, w , it will be given by

$$w = \frac{p_\phi}{\rho_\phi} = \frac{(1/2)\dot{\phi}^2 - V(\phi)}{(1/2)\dot{\phi}^2 + V(\phi)}. \quad (8)$$

This equation shows that, in order to have a dark energy equation of state close to -1 , the field's evolution has to be potential dominated, such that $\dot{\phi}^2 \ll V(\phi)$. This is why, generically, quintessence models are associated to scalar fields slowly evolving in the respective potentials. This can be ensured, for instance, by the slow-roll conditions given by equations (1) and (2).

The scalar field equation of motion is given by the Euler-Lagrange equation

$$\ddot{\phi} + 3H\dot{\phi} + \frac{dV}{d\phi} = 0. \quad (9)$$

Through this equation we can see that the field will evolve in the potential $V(\phi)$ rolling towards a minimum in the quintessence potential, while its motion is damped by the presence of the Hubble parameter, H . Considering a flat Universe, with the FRW metric, the Hubble parameter, as a function of the scale factor a , is given by

$$H^2 = \frac{\rho_T}{3}, \quad (10)$$

where ρ_T is the Universe's total energy density. We will be considering a Universe consisting of pressureless matter and a scalar field playing the role of dark energy. This

implies that $\rho_T = \rho_m + \rho_\phi$. As a function of the scale factor, $\rho_m = \rho_{m0}a^{-3}$, where ρ_{m0} is the present-day value of the matter density; the field's energy density will be given by ρ_ϕ in Eq. (7). In a flat Universe, the present-day value of the matter energy density is determined by $\Omega_{m0} = 1 - \Omega_{\phi0}$, where Ω_{m0} and $\Omega_{\phi0}$ are the ratios of the present-day values of the matter and dark energy densities to the critical density, ρ_c .

A. Model I

The first model we consider is that of a scalar field rolling close to a stable non-zero minimum of its potential. The field is assumed to evolve in a potential that satisfies the slow-roll condition of equation (1), while the other slow-roll condition is somewhat relaxed since $(1/V)d^2V/d\phi^2$ can be large, namely as a result of the curvature at the potential's minimum. This model was extensively studied in [22], where a set of solutions for the evolution of the field was derived, as well as the respective equation of state, $w(a)$, as a function of the scale factor a . These solutions are applicable to a wide array of potentials with non-zero minima, and depend on the present-day values of w and Ω_ϕ , and on the curvature of the potential at the minimum, controlled by the parameter K^2 . The latter is given by equation (19) in [22], which we reproduce here:

$$K^2 = 1 - \frac{4}{3} \frac{V''(\phi_*)}{V(\phi_*)}, \quad (11)$$

where $V''(\phi_*)$, each prime representing a derivative with respect to the scalar field, and $V(\phi_*)$ are, respectively, the curvature and potential values at the minimum of the potential, ϕ_* . The latter corresponds to the present-day value of the dark energy density, $V(\phi_*) = \rho_{\phi0}$. For this model we have $V''(\phi_*) > 0$, which means that $-\infty \leq K^2 \leq 1$. There are three cases of interest: $K^2 = 1$, $0 < K^2 < 1$ and $K^2 < 0$. The limiting case of $K^2 \rightarrow 1$, therefore with zero curvature, was considered in [23] where it was shown that w decreases monotonically with a , a behavior qualitatively similar to that obtained for $w(a)$ in [20] and [21] for a quintessence field in a nearly flat potential and a scalar field rolling near a local maximum of the potential, respectively. For $0 \leq K^2 < 1$, the behavior of $w(a)$ also consists of a slow and monotonic increase in w .

In the case of $K^2 < 0$, the behavior of $w(a)$ is oscillatory, and can be analytically approximated through a combination of sinusoidal functions [22]. For this to happen, we need to have $V''(\phi_*)/V(\phi_*) > 3/4$, requiring the potential to be significantly curved at its minimum. Here, we won't be using the analytical approximation for $w(a)$ derived in [22], but instead calculate w directly from equation (8) by numerically solving equation (9) as a function of a . This will depend on three parameters: $\Omega_{\phi0}$, K^2 and the initial value for the field, ϕ_i . The field's

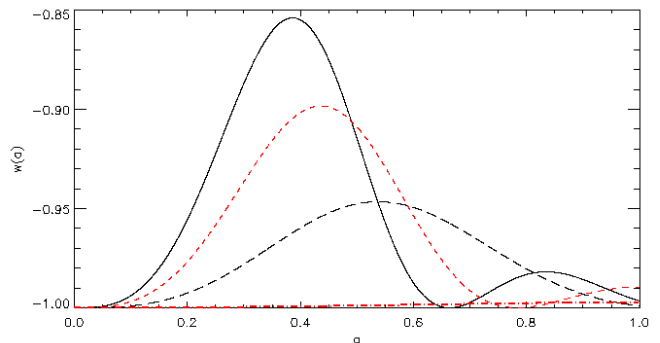


FIG. 1. Evolution of w for Model I, assuming different values of K^2 : $K^2 = 0$ (dot-dashed red line); $K^2 = -10$ (long dashed black line); $K^2 = -20$ (short dashed red line), and $K^2 = -30$ (solid black line). The values of $\Omega_{\phi0}$ and ϕ_i were fixed at 0.74 and 0.30, respectively.

initial velocity, $\dot{\phi}$ is assumed to be zero, which determines the initial value of the equation of state to be -1 . Also, we will be assuming a quadratic potential, such that

$$V(\phi) = \rho_{\phi0} + V_2\phi^2, \quad (12)$$

where V_2 is the curvature at the minimum, determined by $V_2 = (3/8)(1 - K^2)\rho_{\phi0}$.

In Fig. 1 we show examples of the evolution of $w(a)$ for different values of K^2 , with $\Omega_{\phi0}$ and ϕ_i kept fixed, and $H_0 = 70 \text{ km s}^{-1} \text{ Mpc}^{-1}$. We can see that w evolves monotonically for $K^2 = 0$. As the value of K^2 becomes negative and increases in absolute value, the potential becomes more curved at the minimum, and w exhibits a more dynamical behavior. For these negative K^2 values, the field is actually able to significantly overcome the Hubble friction term and cross the potential's minimum, oscillating around it with decreasing amplitude. This is reflected in the equation of state in the form of maxima with decreasing amplitude located between points where the field's motion comes to a halt, which happens when the field reaches the maximum height it possibly can on the potential. As the curvature at the minimum of the potential, and thus K^2 , gets larger, the oscillatory behavior becomes more evident, due to a decrease in the amount of time required to complete a full oscillation about the minimum. However, note that if $\phi_i = 0$, then, whichever values the other parameters might take, no oscillations occur, and the field effectively behaves as a cosmological constant.

B. Model II

The second model we consider is that of a scalar field oscillating around zero, with a potential of the form [27]

$$V(\phi) = \frac{m^2 M^2}{2} \left[\frac{(\phi/M)^2}{1 + (\phi/M)^{2(1-\alpha)}} \right]. \quad (13)$$

This potential is very flat for small field values, **acquiring** a quadratic form for large field values, so that

$$V(\phi) \approx \begin{cases} (m^2 M^2/2) (\phi/M)^{2\alpha} & \phi \gg M, \\ (m^2/2) \phi^2 & \phi \ll M. \end{cases} \quad (14)$$

The scale m determines the curvature of the potential at the minimum, $V''(0)$, whereas the scale M determines where the potential changes shape and enters the quadratic region, where the field will eventually oscillate. This model allows, if certain conditions are met, to have a field slowly-rolling until recently and then present some oscillatory behavior close to the present.

It has been show that for a power-law potential, $V(\phi) \propto |\phi|^n$, one obtains $w = (n - 2)(n + 2)$ when averaged over the oscillation period, T , as long as it is much smaller than the Hubble time, i.e., $T \ll H^{-1}$ [24–26].

Therefore, in the oscillatory region ($\phi \ll M$) of the potential being considered, w should average to zero, because we then effectively have $V(\phi) \propto |\phi|^2$, i.e. $n = 2$. This means the scalar field would then be behaving like pressureless matter, which goes against the need for having a negative pressure component to drive the cosmic acceleration. However, this model can be fine-tuned so that the oscillatory region of the potential is reached close enough to the present that the predicted large-scale dynamic of the Universe does not deviate much from that expected in a model where it is the presence of a cosmological constant that makes the Universe accelerate [27]. This fine-tuning can be achieved if the parameters of the model being considered take values around $\Omega_{\phi_0} = 0.75$, $m/H_0 = 1130.6$, with H_0 being the present-day value of the Hubble parameter, $M = 0.002$ and $\phi_i/M = 23.7$, where ϕ_i is the initial value of the field. In this particular realization of Model II, the oscillatory behavior only starts around $a = 0.8$, avoiding the appearance of the gravitational instabilities that [28] have shown to be a problem for early rapidly oscillating models with a negative averaged equation of state.

In Fig. 2 we show two examples of the evolution of w in Model II, for $M = 0.0018$ and $M = 0.0022$, with $H_0 = 70 \text{ km s}^{-1} \text{ Mpc}^{-1}$ and all other parameters fixed by the ratios mentioned in the previous paragraph. For larger M , one would expect the field to enter the quadratic region of the potential sooner, meaning oscillations should start at a lower value of a . However, because the ratio ϕ_i/M is kept fixed, an increase in M will lead to a proportionally larger ϕ_i , which by itself would lead to a delay in the start of the oscillatory period. In fact, it is the change in ϕ_i which has the largest impact on the value of a at the beginning of such period, given that, as Fig. 2 shows, increasing M leads to a lower value of a at the start of the oscillatory period. Before entering this

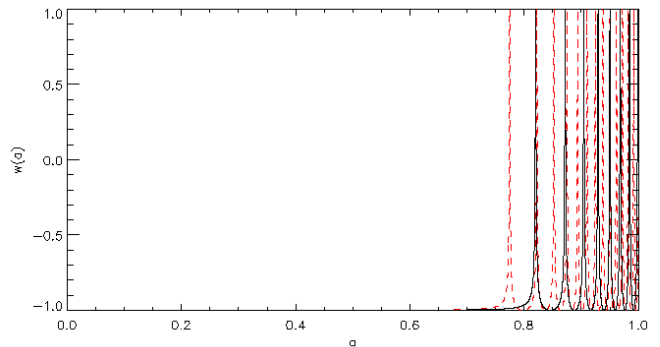


FIG. 2. Evolution of w for Model II, assuming different values of M : $M = 0.0018$ (dashed red line), and $M = 0.0022$ (solid black line). The value of Ω_{ϕ_0} was assumed to be 0.75.

period, the field’s evolution is quite similar in both cases, slowly rolling down the potential with w almost indistinguishable from -1 . As the field enters the quadratic region, it starts to oscillate ever more rapidly around the potential’s zero minimum. We will then have w varying between ± 1 , with a constant averaged value of 0. Thus, the field in effect starts behaving like pressureless matter, with its energy density decreasing as a function of a^{-3} . And, since $V(\phi) = \rho_\phi$ when the field reaches its maximum height on the potential during an oscillation, the field’s oscillation amplitude should decrease with $a^{-3/2}$.

III. EUCLID

The Euclid mission is a medium-class space mission expected to be launched by the European Space Agency in 2020. Its main objective is to help better constrain the large-scale geometry of the Universe and nature of the dark energy and dark matter components of the Universe. More specifically, Euclid aims to enable the measurement of the dark energy parameters w_0 and w_a with 2% and 10% accuracy, respectively [29]. These parameters characterize the dark energy equation through [30]

$$w(a) = w_0 + (1 - a)w_a, \quad (15)$$

where w_0 is the present-day value of w .

The specifications of Euclid were defined so that its main scientific objective can be achieved using the information contained in the Baryonic Acoustic Oscillations (BAO) present in the matter power spectrum and in the Weak Lensing (WL) features of the large-scale distribution of matter [29]. The two cosmological probes will rely mostly on Euclid’s wide survey, although they will require substantially different sets of data: spectroscopic for BAO and photometric for WL. The Euclid wide survey will cover an area of at least 15000 deg^2 , restricted to galactic latitudes $|b| > 30^\circ$, and will be able to measure

the shapes and redshifts of galaxies up to a redshift of $z \approx 2$, with a median redshift of approximately 1 [29].

A. Baryonic Acoustic Oscillations

In the early stages of our Universe, before the recombination era, its composition consisted of a dense and hot plasma where photons and baryons were coupled. This primordial plasma struggled between the possibility of a gravitational collapse and the repulsion of the outward electromagnetic and kinetic pressures. These two competing effects led to the formation of acoustic waves in the photon-baryon fluid, whose signature is still imprinted both in the cosmic microwave background radiation (CMB) and in the large-scale distribution of matter (BAO). Namely, a series of peaks in the CMB angular power spectrum and in the galaxy power spectrum, with a characteristic scale, the sound horizon at recombination, s , which can be accurately measured using present CMB data, such as that acquired by WMAP [31]. Its identification, both in the transverse, y , and radial, y' , directions using the galaxy power spectrum, then allows the comoving distance, $\chi(z)$, and the Hubble parameter, $H(z)$, as a function of redshift, to be constrained, given that [32]

$$y = \frac{\chi(z)}{s} \quad (16)$$

and

$$y' = \frac{c}{H(z)s}. \quad (17)$$

In order to assess the constraining power of the BAO method applied to Euclid's spectroscopic survey with respect to the parameters that will be varied in the two quintessence models we are considering, we will use the iCosmo software package [33] to determine the Fisher matrix associated to this survey. The Fisher matrix is a useful tool for planning future observations, as the diagonal elements of its inverse indicate the best possible constraints that can be achieved for the assumed free parameters, according to the Cramer-Rao theorem [34]. The Fisher matrix associated with the BAO method, when the available information allows for the estimation of the two characteristic acoustic scales y and y' , is given by [35]

$$F_{\alpha\beta}^{BAO} = \sum_i \frac{1}{y(z_i)^2 x_i^2} \frac{\partial y(z_i)}{\partial p^\alpha} \frac{\partial y(z_i)}{\partial p^\beta} + \sum_i \frac{1}{y'(z_i)^2 x_i'^2} \frac{\partial y'(z_i)}{\partial p^\alpha} \frac{\partial y'(z_i)}{\partial p^\beta}, \quad (18)$$

where the sums run over the observational bins at different redshifts z , p^α represents the parameter with respect to which the partial derivative is taken, while x and x'

represent the relative errors associated to the measurements of the transverse and radial scales, respectively. We note that iCosmo uses the analytical approximation of [36] to evaluate the expected accuracy of an experiment's measurement of the BAO scales.

In our calculation of the constraints imposed on the free parameters of the two quintessence models being considered, using the BAO method, we assumed the galaxy redshift distribution of Euclid's spectroscopic wide survey to be that in [37], for a limiting flux of 3×10^{-6} erg s $^{-1}$ cm $^{-2}$. We also assumed a median redshift of 1.1, a redshift measurement error of $\Delta z = 0.001(1+z)$ and a redshift range of [0.4, 2.2] distributed over 14 redshift bins, following [29].

B. Weak Lensing

Weak Lensing is a subtle gravitational lensing effect, caused by the slight deflection of the light emitted by distant galaxies due to the existing matter distribution along their line of sight. This will lead to changes in the perceived galaxy shapes. For instance, a galaxy that is intrinsically circular could appear to us as elliptical. Such type of distortion can be approximated to first order through a simple matrix transformation [38, 39]

$$\begin{pmatrix} x_2 \\ y_2 \end{pmatrix} = \begin{pmatrix} -\kappa - \gamma_1 & -\gamma_2 \\ -\gamma_2 & -\kappa + \gamma_1 \end{pmatrix} \begin{pmatrix} x_1 \\ y_1 \end{pmatrix}. \quad (19)$$

The components γ_1 and γ_2 form the complex shear, equal to $\gamma_1 + i\gamma_2$. A positive γ_1 stretches the image along the x direction and compresses it on the y direction, γ_2 has the same effect, but respectively along the $y = x$ and $y = -x$ directions, while κ is the convergence, measuring the dilatation or contraction of the observed image. The pair of coordinates (x_1, y_1) and (x_2, y_2) denote points on the observed image and on the source, respectively. The magnitude of the lensing signal depends both on the amount of matter along the line of sight, and on the distances between the observer, the lens and the source. This makes weak lensing ideal for measuring the Universe's mass distribution and geometry and, therefore, for constraining cosmological parameters, such as those that can be used to characterize the dark energy.

We again use the iCosmo software [33] to forecast the constraining power of Euclid's WL survey with respect to the parameters that will be varied in the two quintessence models under consideration. Euclid will use a weak lensing technique known as tomography: the galaxies in Euclid's wide survey will be divided into separate (photometric) redshift bins, with the two-point correlation function of the shear field computed by looking at the shear patterns in each bin and between different bins. The corresponding cross-power spectrum between bins i and j characterized through the coefficients $C_{ij}(l)$, where l is the order of the multipole moment. The Fisher matrix

associated with weak lensing tomography is then given by [33, 40, 41]

$$F_{\alpha\beta}^{WL} = \sum_l \frac{2l+1}{2} f_{sky} \frac{\partial C_{ij}(l)}{\partial p^\alpha} [C_l]_{jk}^{-1} \frac{\partial C_{km}(l)}{\partial p^\beta}, \quad (20)$$

where again p^α represents the parameter with respect to which the partial derivative is calculated, and f_{sky} is the fraction of the sky covered by the survey. The covariance matrix, $[C_l]_{ij}^{-1}$, for a given l for the $i-j$ bin pair, can be written as [40, 41]

$$[C_l]_{ij}^{-1} = \left[C_{ij}(l) + \frac{\gamma_{int}^2}{N_g} \delta_{ij} \right]^2, \quad (21)$$

where γ_{int} is the random mean-square intrinsic shear in one component, δ_{ij} is the Kronecker symbol and N_g is the number density of galaxies in the i -th bin.

The coefficients that characterize the shear cross-power spectrum between redshift bins i and j , $C_{ij}(l)$, are given by [40–42]

$$C_{ij}(l) = \int_0^\infty dz \frac{W_i(z)W_j(z)}{\chi(z)^2 H(z)} P_\delta \left(\frac{l}{\chi(z)}, z \right), \quad (22)$$

where only the Fourier modes with $l = k\chi$ are assumed to contribute to the integral. $W(z)$ are window functions (also known as lensing efficiency functions), dependent on geometric factors, and P_δ is the three-dimensional matter density power spectrum at redshift z , which depends on how fast is the growth of the density perturbations in the matter distribution.

Assuming that the Universe contains only photons, baryons, cold dark matter and a quintessence scalar field, as long as this last component does not dominate the total energy density of the Universe at early times, namely before recombination, the Eisenstein & Hu transfer function [43] can be used to determine the power spectrum of the initial matter density perturbations. In order to infer the non-linear corrections to the evolving linear power spectrum, we used the HALOFIT model [44], although this may lead to some loss of precision in our results since, as showed in [45], use of the HALOFIT model in dark energy models with evolving w requires suitable corrections if one is interested in an accurate estimate of the non-linear corrections to the linear power spectrum.

Following [29], we assume the Euclid weak lensing photometric survey will measure the shape of over 2 billion galaxies at a median redshift of 0.9, covering a redshift range between $0 < z < 2$ distributed over 10 redshift bins in a 15.000 deg² sky. For calculation purposes, the assumed number of galaxies per arcmin² is 30. The galaxy redshift distribution is expected to be close to that given by the analytical formula of [46], with parameters $\alpha = 2$ and $\beta = 1.5$ [40, 41]. The photometric redshift measurement error is assumed to be $\Delta z/(1+z) = 0.05$, while

γ_{int} was taken to be 0.22 [41]. The multipole range used in the analysis is limited to $\ell_{\max} = 5000$ to minimize the effects of baryonic feedback on the power spectrum [47].

We should point out that, in our calculations, we have neglected the effect of intrinsic alignments. Hence our forecasts are optimistic in that sense.

IV. RESULTS

In this section, we present the results for Euclid's expected constraints on the parameters of the quintessence models under consideration. Given that there aren't a priori theoretically preferred values for these parameters, we will set their fiducial values to those that maximize the joint posterior probability distribution of the parameters given the most recent data available from the Supernova Cosmology Project (SCP) [48].

A. Fiducial parameter combinations

Supernovae type Ia are standard candles, since they reach essentially the same luminosity at their peak brightness. The ratio of this constant peak luminosity to the measured flux is proportional to the luminosity distance squared. If we also know the redshift at which a supernova occurs, we can then determine the relation between co-moving distance and redshift, which carries information on all the cosmological parameters that affect it. Namely, those that characterize the quintessence models we are considering.

Assuming that, in each of the quintessence models being considered, all possible values for the free parameters have equal prior probability, then the joint posterior probability distribution of the parameters for each model is proportional to the likelihood of the most recent SCP data. This is provided as

$$\mu(z) \equiv m - M, \quad (23)$$

where z , m and M are, respectively, the redshift, (measured) apparent and (assumed) absolute magnitudes of the observed supernovae. The quantity $\mu(z)$ is related to the cosmology-dependent luminosity distance, d_L (in parsecs), through

$$\mu(z) = 5 \log_{10} d_L - 5. \quad (24)$$

Given that the uncertainty associated with the SCP estimates of $\mu(z)$ is assumed to be well characterized through a Gaussian probability distribution, the likelihood of the most recent SCP data is then proportional to the exponential of $-\chi^2/2$, where [49]

$$\chi^2 = \sum_{i,j} [f_i(p) - \mu_i(z_i)] [E^{-1}]_{ij} [f_j(p) - \mu_j(z_i)]. \quad (25)$$

with the $\mu_i(z_i)$ and E^{-1} representing, respectively, the SCP data and the inverse of its covariance matrix, which includes systematic uncertainties. The $f_i(z_i, p)$ are the theoretically expected values for the μ_i , assuming the measured redshift z_i and the set of parameters p for the model f to be true.

For the Model I, we have allowed $\Omega_{\phi 0}$, ϕ_i and K^2 to vary freely within the intervals $[0.70, 0.80]$, $[0.0, 1.0]$ and $[-50.0, 0.0]$, respectively. In the case of Model II, we have allowed $\Omega_{\phi 0}$ and M to vary freely within the intervals $[0.60, 0.80]$ and $[0.0180, 0.00220]$, respectively. The interval allowed for M , as well as the conditions $\phi_i = 23.7 M$ and $m = 1130.6 H_0^{-1}$, were set to force the scalar field to only starts oscillating around $a = 0.8$, rendering the model viable as discussed before. The present-day value of the Hubble parameter was always assumed to be $H_0 = 70 \text{ km s}^{-1} \text{ Mpc}^{-1}$. For each model, the combination of parameters that maximizes the likelihood of the most recent SCP data, and hence the joint posterior given our assumptions of flat priors for the parameters, is

- Model I: $\Omega_{\phi 0} = 0.74$, $K^2 = -15.0$, $\phi_i = 0.30$
- Model II: $\Omega_{\phi 0} = 0.75$, $M = 0.00202$

which we will henceforth take to be our fiducial model parameter sets. We will also always assume to be working on a spatially-flat Universe, thus $\Omega_{m0} = 1 - \Omega_{\phi 0}$, where the power spectrum of primordial adiabatic Gaussian matter density perturbations is approximately scale-invariant $n_s = 1$, the abundance of baryons is taken to be 0.045 and the present-day amplitude of the matter density perturbations smoothed on a sphere with a radius of $8 h^{-1} \text{ Mpc}$ is equal to $\sigma_8 = 0.8$, motivated by the WMAP-7 results [13, 31]. Fig. 3 shows that the recent evolution of the Hubble parameter, H , as a function of redshift z , for the models we have been considering and assuming the fiducial parameters, does not deviate much from the ΛCDM case.

B. Confidence Regions for Euclid

Using the results of last section, we forecast the constraining power that the Euclid mission will have on the models analyzed in this work. For that, we have used the software iCosmo [33], using as input the fiducial values defined before and leaving all other parameters with their default values. We then marginalized over the non interesting parameters and obtained the two dimensional 68% and 95% confidence regions, which we plot here, alongside with the one dimensional distribution for each parameter of interest.

The first figure we present here, Fig. 4, shows the expected 68% and 95% confidence regions obtained for the two quintessence models analyzed in this work, when the Weak Lensing method is applied to Euclid's photometric survey. It is clear that through this survey it will

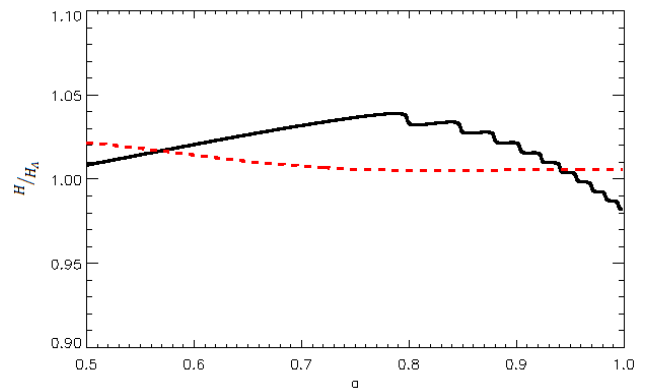


FIG. 3. Recent evolution of the ratio between the Hubble Parameter, $H(a)$, as a function of the scale factor a , evaluated for the fiducial parameters of both models and the corresponding ΛCDM (with $\Omega_{\Lambda} = \Omega_{\phi 0}$). The black (full) and red (dashed) lines correspond to Models I and II, respectively.

be possible to place tight constraints on these particular quintessence models.

On the other hand, Fig. 5, shows the forecasted confidence regions for both models when the BAO method is applied to Euclid's spectroscopic survey. It is clear that through this survey it will not be possible to place as tight constraints on these particular dark energy models as by applying the Weak Lensing method to Euclid's photometric survey, given that the confidence regions are now much wider around the central values of the parameters.

In the case of Model I, a clear negative correlation is found between the preferred values for K^2 and ϕ_i , using both the WL and BAO data. This is expected given that a more negative K^2 would lead to earlier oscillations in the quintessence field, which could be prevented by choosing higher values for ϕ_i . However, interestingly, the relationship between $\Omega_{\phi 0}$ and K^2 (as well as ϕ_i) changes whether its the WL or the BAO data that it is being considered: a positive (negative for ϕ_i) correlation for the first type of data becomes negative (positive for ϕ_i) for the second type of data.

In the case of Model II, there is a positive correlation between the two parameters. In general, the oscillations in the field start sooner both for larger M and $\Omega_{\phi 0}$. However, fixing the ratio ϕ_i/M , to keep the start of the oscillatory period roughly constant, produces the opposite behaviour as discussed earlier on. Hence, an increase of M (and the corresponding decrease of ϕ_i) are compensated by a larger $\Omega_{\phi 0}$ producing thus a positive correlation.

Lastly, Fig. 6, shows the forecasted confidence regions for both models arising from the combined application of the Weak Lensing and BAO methods to the Euclid wide survey. As expected, the combination of the constraints obtained through the two methods considered does not show a great improvement over those resulting from applying just the Weak Lensing method. Tables I and II

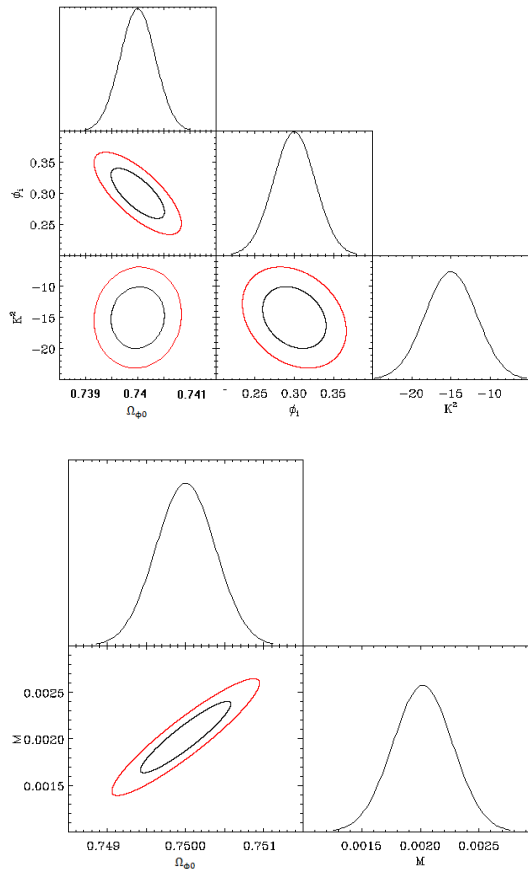


FIG. 4. It is shown the 68% (red line) and 95% (black line) forecasted confidence regions obtained when the Weak Lensing method is applied to Euclid’s photometric survey. The upper panel refers to model I, and the lower panel to model II. For both models, we have assumed as central values the fiducial values determined in the previous section. We also plot the one-dimensional distributions for each parameter.

	Weak Lensing	BAO	Combined
$\Omega_{\phi 0}$	0.000337	0.0312	0.000332
K^2	3.281	51.734	3.190
ϕ_i	0.0267	0.438	0.0262

TABLE I. The 1σ marginalized values for the first model parameters obtained by applying the Weak Lensing and BAO methods, individually and jointly, to Euclid’s wide survey

summarize all the results by presenting the 1σ values for the first and second models parameters, respectively.

V. CONCLUSION

In this paper we considered two quintessence models and determined the expected constraints that the future space mission Euclid will be able to place on them. The chosen models have the particular feature of predicting

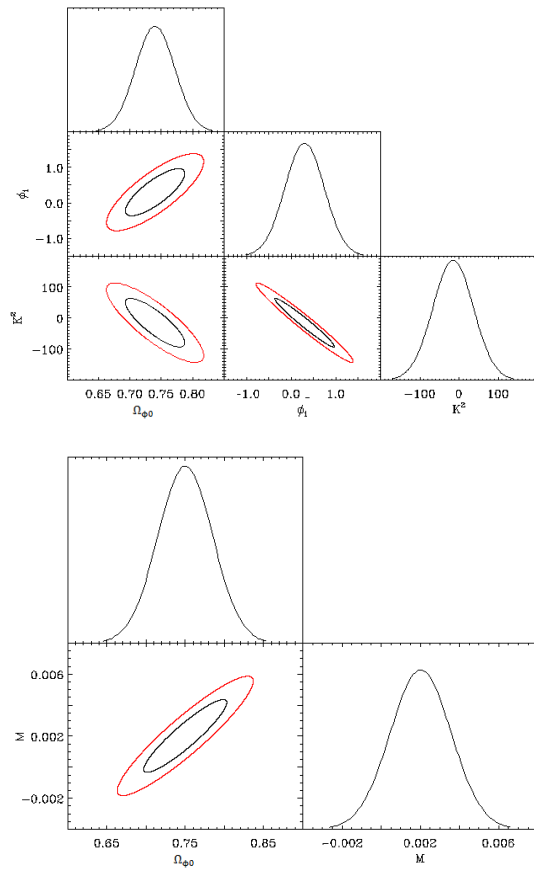


FIG. 5. It is shown the 68% (red line) and 95% (black line) forecasted confidence regions obtained when the BAO method is applied to Euclid’s spectroscopic survey. The upper panel refers to model I, and the lower panel to model II. For both models, we have assumed as central values the fiducial values determined in the previous section. We also plot the one-dimensional distributions for each parameter.

	Weak Lensing	BAO	Combined
$\Omega_{\phi 0}$	0.000380	0.0350	0.000358
M	0.000253	0.00155	0.000236

TABLE II. The 1σ marginalized values for the second model parameters obtained by applying the Weak Lensing and BAO methods, individually and jointly, to Euclid’s wide survey

recently oscillating equations of state, in opposition to the current paradigm of Λ CDM, for which the equation of state takes a constant value of -1 throughout cosmic evolution.

In order to obtain plausible fiducial values for the parameters of the models, we have used the most recent data available from the Supernova Cosmology Project. We performed a statistical analysis, whereby the parameters were allowed to vary within plausible a priori intervals, so that the combination that maximized the joint posterior of the parameters, given the Supernovae data,

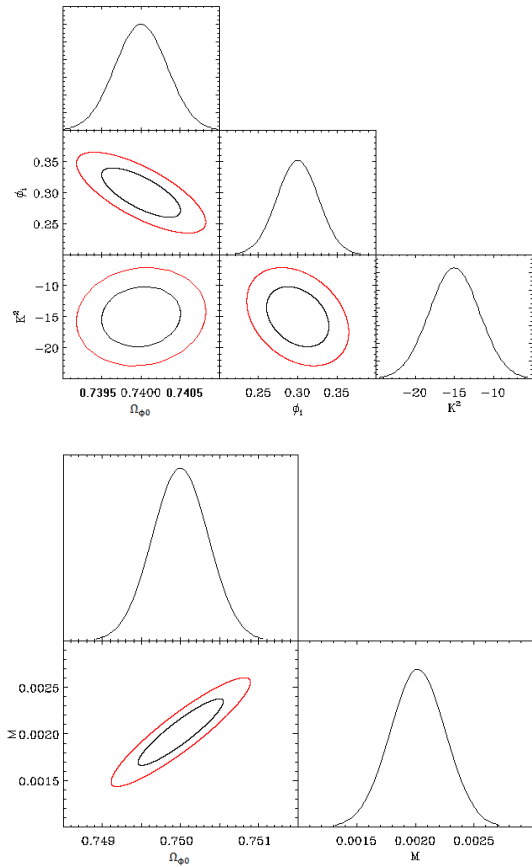


FIG. 6. It is shown the 68% (red line) and 95% (black line) forecasted confidence regions obtained when both the Weak Lensing and BAO methods are applied to Euclid’s wide survey. The upper panel refers to model I, and the lower panel to model II. For both models, we have assumed as central values the fiducial values determined in the previous section. We also plot the one-dimensional distributions for each parameter.

could be estimated. As expected, in both cases we obtained fiducial values for the parameters that lead to an overall expansion history for the Universe quite similar to that of Λ CDM, although the recent evolution of the equation of state in both models is very different with respect to the Λ CDM case.

Then, using the software iCosmo, we have obtained the expected constraints one will be able to place on the quintessence models considered, around the assumed fiducial values, using Euclid data. We concluded that, while applying the Weak Lensing method to Euclid’s photometric survey it will be possible to place tight constraints on these models, the BAO method applied to Euclid’s spectroscopic survey per se will not allow that. In order for the latter to approach the constraining power of the former, one will have to consider the full information contained in the spectroscopically-derived matter power spectrum, $P(k)$, including its full shape, amplitude and redshift distortions, as suggested by forecasts for Euclid using the $w_0 - w_a$ parameters for dark energy [50]. Our results agree with [51], where several oscillating dark energy models were considered, and the conclusion reached was that those oscillations would probably be more easily detectable using Weak Lensing data, rendering this as, possibly, the best approach to constrain the type of models we have been considering.

ACKNOWLEDGEMENTS

We would like to thank Henk Hoekstra and Martin Kunz for their comments on this manuscript.

NAL, PTPV and IT acknowledge financial support from Fundação para a Ciência e a Tecnologia (FCT), respectively, through grant SFRH/BD/85164/2012, project PTDC/FIS/111725/2009, and grant SFRH/BPD/65122/2009. IT also acknowledges support from the European Programme FP7–People and Project CERN/FP/123618/2011.

-
- [1] A. G. Riess *et al.*, *Astron. J.* **116**, 1009 (1998)
 - [2] S. Perlmutter *et al.*, *Astroph. J.* **517**, 565 (1999)
 - [3] A. G. Riess *et al.*, *Astroph. J.* **659**, 98 (2006)
 - [4] D. N. Spergel *et al.*, *Astroph. J. Suppl.* **170**, 377 (2007)
 - [5] L. Amendola *et al.*, arXiv:1206.1225 (2012)
 - [6] L. Amendola, D. Polarski, R. Gannouji, and S. Tsujikawa, *Phys. Rev. D* **75**, 083504 (2007)
 - [7] T. Clifton, P. G. Ferreira, A. Padilla, and C. Skordis, *Physics Reports* **513**, 1 (2012)
 - [8] R. Maartens, *Living Rev. Rel.* **7**, 7 (2004)
 - [9] D. J. Eisenstein *et al.*, *Astroph. J.* **633**, 560 (2005)
 - [10] M. Kowalski *et al.*, *Astroph. J.* **686**, 749 (2008)
 - [11] R. Kessler *et al.*, arXiv:0908.4274v1 (2009)
 - [12] G. Hinshaw *et al.*, arXiv:1212.5226 (2013)
 - [13] O. Lahav and A. R. Liddle, arXiv:1002.3488v1 (2010)
 - [14] T. Padmanabhan, *Phys. Rept.* **380**, 235 (2003)
 - [15] B. Ratra and P. J. E. Peebles, *Phys. Rev. D* **37**, 3406 (1988)
 - [16] M. S. Turner and M. White, *Phys. Rev. D* **56**, 4439 (1997)
 - [17] R. R. Caldwell, R. Dave, and P. J. Steinhardt, *Phys. Rev. Lett.* **80**, 1582 (1998)
 - [18] I. Zlatev, L. Wang, and P. J. Steinhardt, *Phys. Rev. Lett.* **82**, 896 (1999)
 - [19] A. Mazumdar, arXiv:1106.5408v1 (2011)
 - [20] R. J. Scherrer and A. A. Sen, *Phys. Rev. D* **77**, 083515 (2008)
 - [21] S. Dutta and R. J. Scherrer, *Phys. Rev. D* **78**, 123525 (2008)
 - [22] S. Dutta, E. N. Saridakis, and R. J. Scherrer, *Phys. Rev. D* **79**, 103005 (2009)
 - [23] T. Chiba, *Phys. Rev. D* **79**, 083517 (2009)
 - [24] M. S. Turner, *Phys. Rev. D* **28**, 1243 (1983)
 - [25] J.-A. Gu, arXiv:0711.3606v1 (2007)
 - [26] S. Dutta and R. J. Scherrer, *Phys. Rev. D* **78**, 083512 (2008)

- (2008)
- [27] M. A. Amin, P. Zukin, and E. Bertschinger, arXiv:1108.1793v1 (2011)
- [28] M. C. Johnson and M. Kamionkowski, Phys. Rev. D **78**, 063010 (2008)
- [29] R. Laureijs *et al.*, arXiv:1110.3193 (2011)
- [30] E. V. Linder, Phys. Rev. D **90**, 091301 (2003)
- [31] C. L. Bennett *et al.*, arXiv:1212.5225 (2013)
- [32] B. A. Bassett and R. Hlozek, arXiv:0910.5224 (2009)
- [33] A. Refregier *et al.*, arXiv:0810.1285v2 (2011)
- [34] M. Tegmark, A. N. Taylor, and A. F. Heavens, Astroph. J. **480**, 22 (1997)
- [35] D. Parkinson *et al.*, Mon. Not. Roy. Astron. Soc. **377**, 185 (2007)
- [36] C. Blake *et al.*, Mon. Not. Roy. Astron. Soc. **365**, 255 (2006)
- [37] J. E. Geach *et al.*, Mon. Not. Roy. Astron. Soc. **402**, 1330 (2010)
- [38] A. Refregier, Ann. Rev. of Astron. and Astroph. **41**, 645 (2003)
- [39] H. Hoekstra and B. Jain, Ann. Rev. Nucl. Part. Sci. **58**, 99 (2008)
- [40] S. Camera, C. Carbone, and L. Moscardini, arXiv:1202.0353v3 (2012)
- [41] A. B. Belloso, J. García-Bellido, and D. Sapone, arXiv:1105.4825v2 (2011)
- [42] W. Hu, Astroph. J. **522**, L21 (1999)
- [43] W. Hu and D. J. Eisenstein, Astroph. J. **496**, 605 (1998)
- [44] R. E. Smith *et al.*, Mon. Not. Roy. Astron. Soc. **341**, 1311 (2003)
- [45] P. McDonald, H. Trac, and C. Contaldi, Mon. Not. Roy. Astron. Soc. **366**, 547 (2006)
- [46] I. Smail *et al.*, Mon. Not. R. Astron. Soc. **270**, 245 (1994)
- [47] E. Somboloni *et al.*, Mon. Not. R. Astron. Soc. **417**, 2020 (2011)
- [48] S. C. Project, <http://supernova.lbs.gov>
- [49] G. Phil, *Bayesian Logical Data Analysis for the Physical Sciences* (Cambridge University Press, 2005)
- [50] R. Scaramella *et al.*, in *Proceedings of Widefield science and technology for the SKA* (2009)
- [51] F. Pace, C. Fedeli, L. Moscardini, and M. Bartelmann, Mon. Not. Roy. Astron. Soc. **422**, 1186 (2012)